Extreme Mechanics Letters 9 (2016) 353–358

Contents lists available at ScienceDirect

Extreme Mechanics Letters

journal homepage: www.elsevier.com/locate/eml

Mechanical integrity of solution-processed perovskite solar cells

Nicholas Rolston [a], Brian L. Watson [b], Colin D. Bailie [b], Michael D. McGehee [b], João P. Bastos [c], Robert Gehlhaar [c], Jueng-Eun Kim [d], Doojin Vak [d], Arun Tej Mallajosyula [e], Gautam Gupta [e], Aditya D. Mohite [e], Reinhold H. Dauskardt [b,*]

[a] Department of Applied Physics, Stanford University, Stanford, CA, USA
[b] Department of Materials Science and Engineering, Stanford University, Stanford, CA, USA
[c] IMEC, v.z.w., Kapeldreef 75, B-3001 Leuven, Belgium
[d] Commonwealth Scientific and Industrial Research Organisation (CSIRO) Manufacturing, Bayview Avenue, Clayton VIC 3169, Australia
[e] Materials Physics and Application Division, Los Alamos National Laboratory, Los Alamos, NM 87545, USA

ARTICLE INFO

Article history:
Received 10 March 2016
Received in revised form
17 June 2016
Accepted 19 June 2016
Available online 27 June 2016

Keywords:
Perovskite solar cells
Thermomechanical reliability
Grain boundaries
Degradation modes
Fracture processes

ABSTRACT

Low-cost solar technologies such as perovskite solar cells are not only required to be efficient, but durable too, exhibiting chemical, thermal and mechanical stability. To determine the mechanical stability of perovskite solar cells, the fracture resistance of a multitude of solution-processed organometal trihalide perovskite films and cells utilizing these films were studied. The influence of stoichiometry, precursor chemistry, deposition techniques, and processing conditions on the fracture resistance of perovskite layers was investigated. In all cases, the perovskites offered negligible resistance to fracture, failing cohesively below 1.5 J/m^2. The solar cells studied featured these perovskites and a variety of organic and inorganic charge transporting layers and carrier-selective contacts. These ancillary layers were found to significantly influence the overall mechanical stability of the perovskite solar cells and were repeatedly the primary source of mechanical failure, failing at values below those measured for the isolated fragile perovskite films. A detailed insight into the nature of perovskite and perovskite solar cell fracture is presented and the influence of grain size, device architecture, deposition techniques, environmental variables, and molecular additives on these fracture processes is reported. Understanding the influence of materials selection, deposition techniques and processing variables on the mechanical stability of perovskite solar cells is a crucial step in their development.

1. Introduction

The remarkable optoelectronic properties of organohalide-lead perovskite materials show resilience to defects and grain boundaries and hold tremendous promise for low-cost solar cells and next-generation PV [1]. They exhibit efficient photoinduced carrier generation, long carrier lifetimes, high carrier mobilities and internal quantum efficiencies while absorbing strongly over a broad region of the solar spectrum [2]. This optoelectronic resilience enables high conversion efficiencies to be achieved from materials deposited by a wide variety of fabrication techniques, many of which satisfy the requirements for low cost cell manufacturing [3]. Solution-based methods such as spin-coating, slot-die coating, and blade coating are compatible with cheap, plastic substrates in ambient conditions and enable pathways towards large-scale manufacturability [4–10]. However, little is known about the mechanical properties of these perovskite materials and the influence of these same defects and grain boundaries on their thermomechanical reliability.

Our goal has been to provide the field with a much needed metric by which progress in the improvements of the mechanical stability of perovskite solar cells can be evaluated. Fracture of perovskite solar cells is an essential consideration in the goal of increasing their operational lifetime. For perovskites, a fracture not only leads to a loss of ohmic contact, but creates an accelerated pathway for the diffusion of volatile compounds. Accordingly, a fracture will promote degradation through the ingress of moisture or through loss of volatile organics like methylamine or formamide. It was recently reported that hybrid organometal trihalide perovskites exhibit surprisingly high coefficients of thermal

* Correspondence to: Department of Materials Science and Engineering, Stanford University, Stanford, CA 94305-2205, USA. Fax: +1 650 725 4034.
E-mail address: dauskardt@stanford.edu (R.H. Dauskardt).

http://dx.doi.org/10.1016/j.eml.2016.06.006
2352-4316/

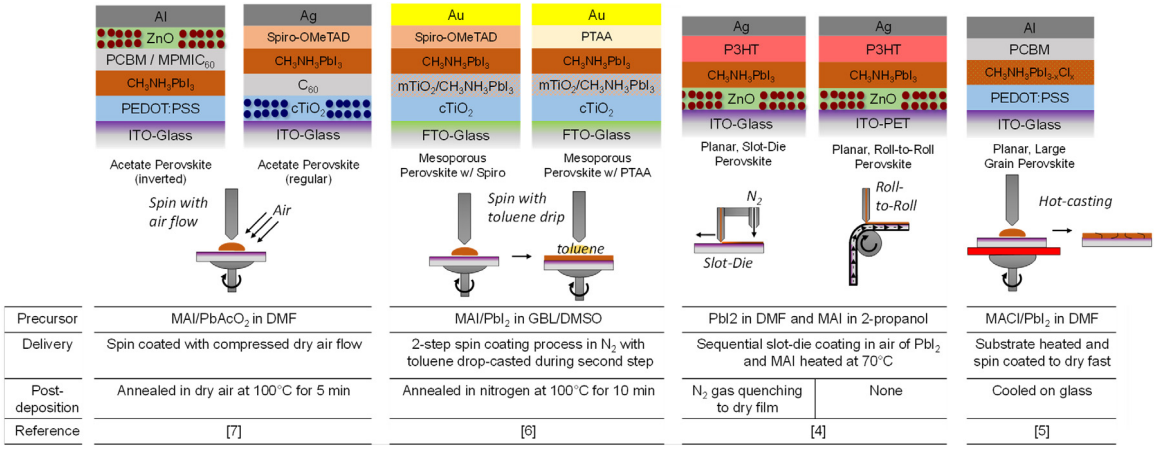

Fig. 1. The various perovskite device architectures and the solution-processing methods used in this study.

expansion, six times higher than soda-lime glass, which would provide a source of stress [11]. Even in the absence of bending stresses and for well-encapsulated devices, mismatch in thermal expansion coefficients can provide sufficient stress through thermal cycling events to induce fracture.

While concerns over the chemical and photo-stability, moisture sensitivity and toxicity of perovskite cells are being addressed [12–15], the thermomechanical properties that impact both the manufacturability and reliability of these cells in field exposures are largely unknown. We have investigated the adhesive and cohesive fracture resistance (G_c) of a wide range of perovskite solar cells sourced through this collaborative effort from across the world. Among all cells studied, the resistance to fracture observed was so low ($G_c < 1.5$ J/m^2), that it could inhibit the success of perovskite solar cells as a viable solar technology. These values are significantly lower than organic solar cells (~5–15 J/m^2) generally recognized to be thermomechanically fragile and competing CIGS (~10 J/m^2) and c-Si cells (~10–200 J/m^2) [16]. For the promises of perovskite photovoltaics to be realized, advances in the understanding of their thermomechanical properties along with the development of materials strategies to address mechanical instabilities are needed.

In this work, the fracture resistance of an array of perovskite solar cells in which the active perovskite layers have been deposited from the solution state by either spin or slot-die coating have been determined. The range of cells also features a variance in the chemistry used to form the perovskite layer, which include the acetate method [7], the mesoporous method [6], the planar method with Spiro-OMeTAD [8], the slot-die method [4], and the large grain method [5]. Cells were fabricated in both conventional and inverted architectures and feature a variety of hole and electron-transporting materials. Fig. 1 shows the different solar cells that were studied in this work indicating the architecture, deposition method and chemistry, the hole and electron transporting layers and carrier-selective contacts. All contacts were thermally or e-beam evaporated and all charge transport layers and perovskite layers were spin coated, except for those deposited by the slot-die method.

2. Experimental

2.1. Adhesion and cohesion testing

Double cantilever beam (DCB) specimens were fabricated with glass or polymethyl methacrylate (PMMA) beams and a thin, room-temperature cured epoxy loaded under displacement control in a thin-film cohesion testing system (Delaminator DTS, Menlo Park, CA) from which a load, P, versus displacement, Δ, curve was recorded. The fracture energy, G_c (J/m^2), was measured in terms of the critical value of the applied strain energy release rate, G. G_c can be expressed in terms of the critical load, P_c, at which crack growth occurs, the crack length, a, the plain strain elastic modulus, E', of the substrates and the specimen dimensions; width, b and half-thickness, h. G_c was calculated from Eq. (1) [17]:

$$G_c = \frac{12P_c^2a^2}{b^2E'h^3}\left(1 + 0.64\frac{h}{a}\right)^2. \quad (1)$$

An estimate of the crack length was experimentally determined from a measurement of the elastic compliance, $d\Delta/dP$, using the compliance relationship in Eq. (2):

$$a = \left(\frac{d\Delta}{dP} * \frac{bE'h^3}{8}\right)^{1/3} - 0.64 * h. \quad (2)$$

All G_c testing was carried out in laboratory air environment at ~25 ° C and ~40% R.H.

2.2. Characterization of the fracture path

Following fracture testing, a survey x-ray photo spectroscopy (XPS, PHI 5000 Versaprobe) scan (0–1100 eV) was made of each of the fractured specimens using monochromatic Al K_α x-ray radiation at 1487 eV in order to characterize the surface chemistry and to help precisely locate the failure path. The specimen half containing the metal electrode is referred to as the "metal side", and the other half including the ZnO is referred to as the "ZnO side". Detailed high-resolution XPS scans were made for compositional analysis and further identification of the fracture path.

Optical and atomic force microscopy (AFM) (XE-70, Park Systems) in non-contact mode were used to characterize the surface morphology and roughness of the fracture path. In addition, phase images were simultaneously collected to reveal further material properties and variations in the surface properties of the fractured cells. Ultraviolet–visible absorption measurements were performed on the ZnO side of fractured cells using an Agilent Cary 6000i UV–Vis–NIR spectrophotometer to determine morphology and reorganization changes in the perovskite cells with exposure.

3. Results and discussion

3.1. Stability of perovskite solar cells

The fracture resistances of the cells determined using the double-cantilever beam test are shown in Fig. 2 as a function of

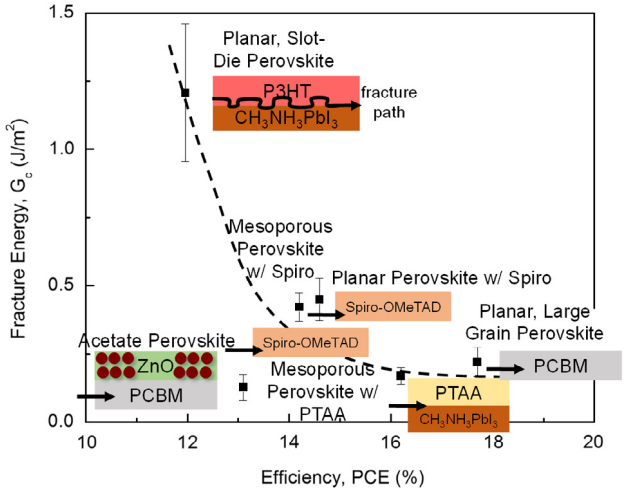

Fig. 2. The measured G_c (J/m^2) and PCE (%) as a function of perovskite device architecture, showing a trade-off between reliability and efficiency. Insets are illustrations of the failure path within the cell structure.

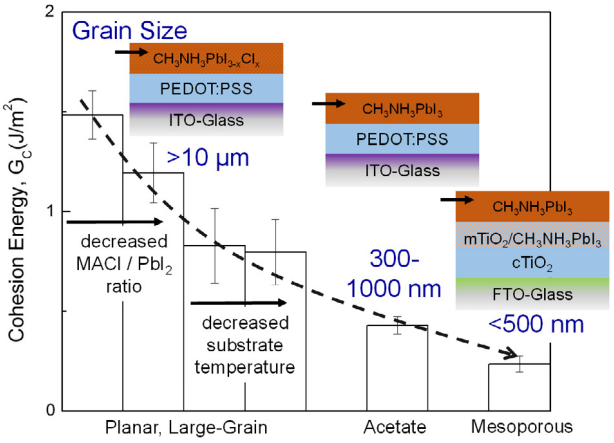

Fig. 3. The measured G_c and PCE as a function of perovskite fabrication method, showing an decrease in cohesion with smaller grain size. Insets are illustrations of the failure path.

the PCE. The results show extremely low G_c values (<1.5 J/m^2) for all cells, indicating that the cells are mechanically fragile. In particular, the charge transport layers currently represent the most fragile elements and are frequently the primary source of failure. In particular, the $PC_{61}BM$ electron-transport layer was the weakest component in large-grain planar cells and acetate cells, fracturing at 0.21 J/m^2 and 0.12 J/m^2 respectively. The hole transport layer was the weakest in mesoporous cells, fracturing in the PTAA layer at 0.17 J/m^2 or in the Spiro-OMeTAD layer at 0.42 J/m^2, depending on which material was used.

Two points of failure were determined for perovskite cells: the adhesion of charge-transporting materials to the perovskite layer (in the case of the planar, slot-die coated method) and the cohesive failure of these auxiliary charge transporting materials (in the case of all other devices). More robust charge transport layers or replacements must be developed that are not mechanically fragile, hydroscopic, corrosive, or susceptible to delamination from perovskite surfaces.

Currently, the most efficient perovskite solar cells utilize organic layers to mediate carrier extraction and charge transport [18]. This places perovskite cells in a similar realm as organic-bulk heterojunction solar cells, which, when subjected to thermo-mechanical analysis, both delaminated readily and exhibited poor layer cohesion [19–22].

3.2. Cohesion of perovskite layers

In order to probe the fracture resistance of the various perovskite layers, test specimens were prepared without the ancillary charge transporting layers that are ordinarily the primary sources of failure. Isolated perovskite layers from each of the fabrication methods shown in Fig. 1 were prepared. The cohesion values of these perovskites are shown in Fig. 3. The G_c values range from 0.24 J/m^2 for mesoporous films to 1.48 J/m^2 for a planar, large-grain film, indicating that once the weak charge transport layers are removed, the perovskites themselves do not exhibit significantly better resistance to fracture. This result is not surprising. Considering the brittle, salt-like crystal structure of these perovskites, one would expect them to exhibit fracture resistances similar to other ionic salts like NaCl, which has a G_c ranging from 0.6 to 1.8 J/m^2 (Figure S1, Appendix A).

We observed that G_c also increases with grain size (Fig. 3). Grain boundaries act as defects that allow for the crack tip to propagate with less resistance. Like many materials, the fracture resistance is a function of the density and distribution of defects and grain boundaries, which relate to the method by which the layer is deposited [23]. It is well known for other crystalline materials and ceramics that defect-laden grain boundaries decrease the cohesion [24]. An increase in the grain size of perovskites from ~500 nm to >10 μm resulted in a six-fold increase in G_c, from 0.24 to 1.48 J/m^2. In large-grain perovskites, the temperatures at which the films are formed and the ratios of precursors used also influenced G_c values. Deviations from the optimum conditions caused G_c to drop to below 0.80 J/m^2. Lower annealing temperatures and MACl/PbI_2 ratios were shown to produce smaller perovskite grains, rougher morphologies, and lower-quality perovskite films that resulted in the observed drop in G_c [5].

3.3. Factors influencing perovskite stability

In addition to grain boundaries, a number of other factors were identified that affect the fracture resistance of perovskites and are of importance when considering design for reliability.

3.3.1. Device architecture

Mesoporous perovskites are effectively reinforced by the embedded metal oxide scaffold and are more robust than planar perovskite films (Figure S2, Appendix A). However, XPS analysis of the fracture surface of this type of perovskite cell revealed that the planar perovskite capping layer that is formed on the top of the mesoporous layer for increased photovoltaic performance is highly susceptible to fracture (Figure S3, Appendix A). The failure of both planar and mesoporous perovskite cells occurred within the pure perovskite layer as shown by the insets in Fig. 3. Previous studies have shown that perovskite devices without any planar capping layer fracture adhesively between the hole-transport layer and the perovskite, which indicates that the TiO_2 scaffold reinforces the perovskite and enhances fracture resistance, deferring failure to the next weakest material or interface [25].

3.3.2. Deposition method

A set of identical planar perovskite devices were made by previously detailed sequential slot die coating method [4]. The procedure uses gas-quenching assisted slot-die coating to form a defect-free PbI_2 layer and convert it to perovskite by depositing MAI solution on top of the slot-die coated PbI_2 at 70 °C. The differences were that one group was prepared on glass substrates by a batch process and another group was prepared on PET substrate by a continuous roll-to-roll process. G_c increased threefold for the glass samples, which fractured at 1.21 J/m^2,

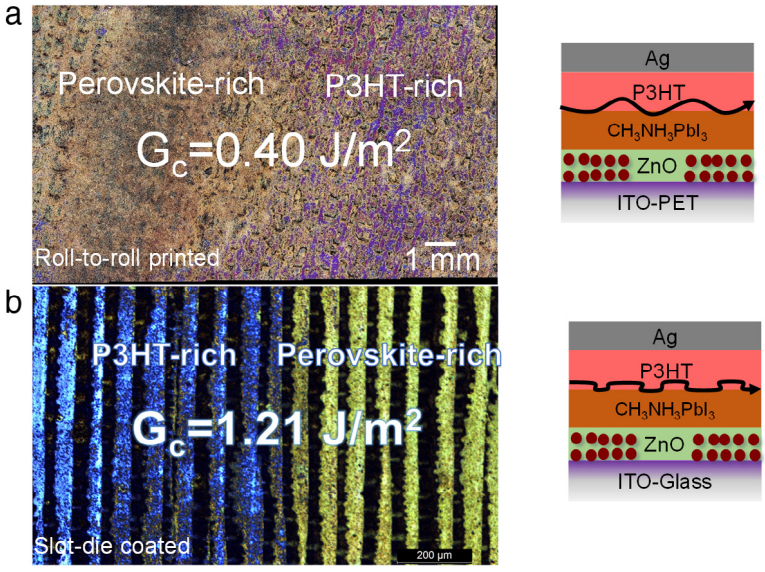

Fig. 4. Optical images of the ZnO side after delamination for planar perovskite devices fabricated on (a) PET and (b) glass.

compared to the weaker PET samples at 0.40 J/m^2 (Fig. 4). The accompanying optical images for the ZnO side of fractured specimens show a marked difference in the morphology of the fracture surfaces, even though the weakest interface was the same for the two different samples. The glass samples show clear striations separated by ∼10–30 μm (Fig. 4(b)), which could be an artifact of the slot-die coater driven by stepper motors.

For the MAI deposition step, the substrates were heated to a coating temperature of 70 °C, which led to rapid solvent drying and created drying lines perpendicular to the coating direction. These striations were not observed on the PET samples prepared by continuous roll-to-roll processing. By controlling the coating conditions, these striations could be exploited to create microstructure and influence fracture resistance.

3.3.3. Exposure conditions

The influence of moisture on the fracture resistance of perovskites was also probed. Unencapsulated, planar perovskite devices were exposed to 55% R.H. at R.T. for up to 24 h to quantify the change in mechanical properties with exposure to water. A decrease in adhesion was observed between the perovskite and hole-transport layer with exposure, and the G_c dropped from 0.40 to 0.18 J/m^2 after 24 h (Fig. 5). AFM phase and topography images of the fractured ZnO side reveal a change in the morphology as a result of this exposure. The failure path transitions from meandering in the P3HT and at the P3HT/perovskite interface in unexposed device to a completely adhesive failure pathway at the P3HT/degraded perovskite interface at the end of exposure. UV–Vis absorption measurements of the ZnO side were taken to further characterize the chemistry, which results in this change through exposure to moisture. The absorption spectrum showed a noticeable decrease in the absorption shoulder at around 600 nm (Figure S4, Appendix A). This shoulder is characteristic of P3HT interchain ordering [26], and the lack of signal after 24 h of exposure indicates that the crack propagated between the P3HT and the degraded perovskite.

A separate batch of planar devices was annealed in a nitrogen atmosphere at 85 °C for 90 h, and a similar decrease in G_c was observed from 0.45 to 0.27 J/m^2 as the Spiro-OMeTAD layer degraded (Figure S5, Appendix A). This decrease in cohesion could occur from Spiro-OMeTAD crystallization during annealing, which has been shown to occur at temperatures below 85 °C [27]. Annealing these devices leads to a rapid decrease in fill factor,

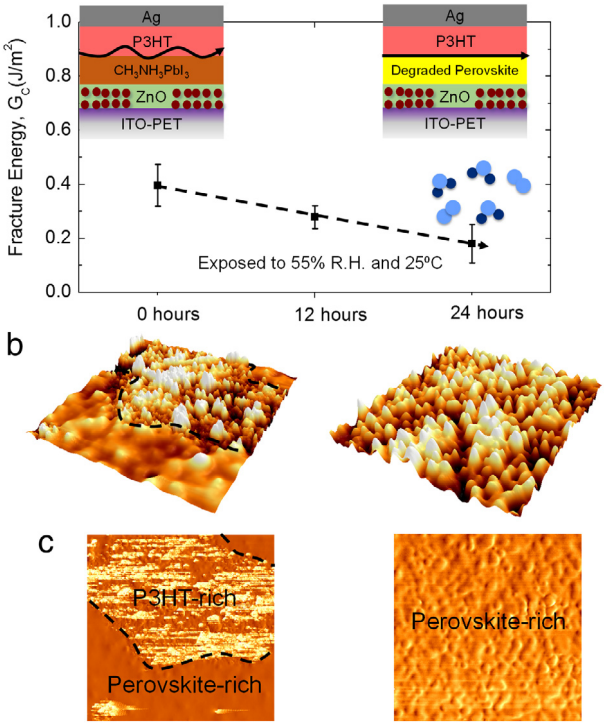

Fig. 5. (a) The measured G_c of planar perovskite cells as a function of exposure time at 55% R.H. and 25 °C. AFM images of the ZnO side after delamination for (b) the topography and (c) the phase, showing the effect of humidity on the fracture surface morphology.

which is an indication of degradation in the transport layer. Identical devices made with PTAA as the hole transport layer do not show such an abrupt performance loss, indicating that the primary degradation mode is the Spiro-OMeTAD and not the perovskite layer.

Perovskite films are also highly susceptible to degradation in electrical properties. Perovskite device efficiencies have been shown to rapidly decrease when exposed to environmental stress parameters such as heat and moisture [28–30]. In the presence of either stress factor, the crystal structure decomposes into PbI_2 and the organic cation is lost: heat leads to thermally induced methylamine evolution and moisture forms a hydrated

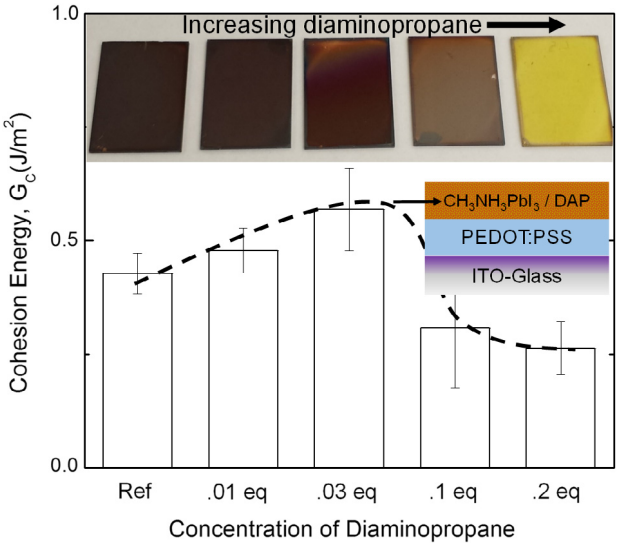

Fig. 6. The measured G_c as a function of crosslinker molar equivalent. The top insets are optical images of the spin coated films after 1-step solution-processing, showing the dramatic effect of increasing linker concentration on perovskite film formation.

phase as methylammonium binds to water. This degradation leads to device failure and presents toxicity hazards because PbI_2 is soluble in water [31]. A connection is observed in the simultaneous degradation of electrical and mechanical properties from environmental effects. Considering the deleterious effects of water on perovskite devices, the importance of fracture resistance in these water soluble materials is heightened. A crack within a bulk perovskite layer provides an accelerated pathway for the ingress of water vapor, and so accelerates the degradation and further moisture-assisted debonding.

3.3.4. Molecular additives

The influence of grain boundaries and size on perovskite layer cohesion suggests that a possible strategy for increasing the fracture resistance of perovskite films would be to reinforce these weak boundaries by cross-linking crystalline domains. Previous work has shown that an increase in the photovoltaic performance and moisture resistance can be achieved when perovskite films are treated with 4-aminobutylphosphonic acid [12]. It was proposed that the ammonium and phosphoric acid termini of this molecule can form interactions with sites at the surface of the perovskite crystals without entering into the lattice. This would effectively strengthen defect-laden grain boundaries [32].

In a control experiment, we probed the influence of a similar molecule, 1,2-diaminopropane, in the synthesis of perovskite films by varying the concentration of diaminopropane in the perovskite precursor solution without changing any of the processing conditions. The amount of 1,2-diaminopropane affected the perovskite film formation. Concentrations of diaminopropane up to 0.03 molar equivalent (eq) compared to $CH_3NH_3PbI_3$ smoothed the morphology of the perovskite and G_c increased from 0.43 to 0.57 J/m^2 (Fig. 6). The linker likely bonded between neighboring perovskite crystal grains to provide structural reinforcement. However, at 0.1 eq the film roughness increased by nearly an order of magnitude, and at 0.2 eq the perovskite was unable to form, resulting in a film of PbI_2 (Figure S6, Appendix A). G_c decreased to below 0.3 J/m^2 at these high linker concentrations from the disruption in perovskite formation and low-quality films. This method shows a proof-of-concept for strengthening perovskite grain boundaries.

4. Implications for reliability

Various factors were identified such as grain boundary engineering, device architecture, deposition method, and molecular additives that can lead to modest improvements in G_c. Consequently, one way to increase perovskite mechanical stability would be to control the fabrication conditions to maximize grain size, incorporate a mesoporous scaffold throughout the entire perovskite layer and then use grain boundary engineering and cross-linkable molecules to minimize the influence of these boundaries on the mechanical properties of the resulting films. It is important to pursue further improvements to intrinsically reinforcing perovskites with small molecules and functionalized polymers with suitable functional groups capable of forming adhesive bonds to perovskite surfaces for the purpose of solvent resistance and chemical stability. A reasonable goal would be to achieve a fracture energy of $\sim$10 J/m^2 for a combination of processing variables, which represents the lower bound of conventional c-Si and CIGS devices.

5. Conclusion

Perovskite solar cells and isolated perovskite films have been shown to exhibit poor resistance to fracture and may be considered to be extremely fragile in the presence of applied loads. The organic charge transport layers present in many of the highest efficiency cells were found to be the primary source of mechanical failure. The influence of defects, grain size, morphology, deposition techniques, environmental conditions, and molecular additives on the failure was studied. Perovskite optoelectronic properties are surprisingly resilient to defects, yet defect-laden samples with an increased number of grain boundaries allow for crack propagation at low fracture resistances. In general, however, factors degrading optoelectronic properties were found to have a similar negative effect on G_c. This work analyzes various factors affecting perovskite mechanical integrity and suggests specific processing conditions to increase cohesion and reliability. Designing thermomechanically robust perovskite cells with longer operational lifetimes is essential for commercialization and long-term feasibility of the technology.

Acknowledgments

This research was supported by the Bay Area Photovoltaics Consortium (BAPVC) (Grant number: DE-EE004946). Part of this work was performed at the Stanford Nano Shared Facilities (SNSF). We thank William. H. Nguyen (Stanford) for helpful discussion. J.-E. Kim and D. Vak were supported by Australian Centre for Advanced Photovoltaics (ACAP) program funded by the Australian Government through the Australian Renewable Energy Agency (ARENA) (Grant number: 6-F023). This work was supported at LANL by Los Alamos Directed Research grant (Program XW11).

Appendix A. Supplementary data

Supplementary material related to this article can be found online at http://dx.doi.org/10.1016/j.eml.2016.06.006.

References

[1] M. Grätzel, The light and shade of perovskite solar cells, Nature Mater. 13 (2014) 838–842. http://dx.doi.org/10.1038/nmat4065.
[2] H.S. Jung, N.G. Park, Perovskite solar cells: From materials to devices, Small 11 (2014) 10–25. http://dx.doi.org/10.1002/smll.201402767.
[3] C.D. Bailie, M.G. Christoforo, J.P. Mailoa, A.R. Bowring, E.L. Unger, W.H. Nguyen, et al., Semi-transparent perovskite solar cells for tandems with silicon and CIGS, Energy Environ. Sci. 8 (2014) 956–963. http://dx.doi.org/10.1039/C4EE03322A.

[4] K. Hwang, Y.S. Jung, Y.J. Heo, F.H. Scholes, S.E. Watkins, J. Subbiah, et al., Toward large scale roll-to-roll production of fully printed perovskite solar cells, Adv. Mater. 27 (2015) 1241–1247. http://dx.doi.org/10.1002/adma.201404598.
[5] W. Nie, H. Tsai, R. Asadpour, A.J. Neukirch, G. Gupta, J.J. Crochet, et al., High-efficiency solution-processed perovskite solar cells with millimeter-scale grains, Science 347 (2015) 522–526.
[6] W.S. Yang, J.H. Noh, N.J. Jeon, Y.C. Kim, S. Ryu, J. Seo, et al., High-performance photovoltaic perovskite layers fabricated through intramolecular exchange, Science (2015) http://dx.doi.org/10.1126/science.aaa9272.
[7] W. Zhang, M. Saliba, D.T. Moore, S.K. Pathak, M.T. Horantner, T. Stergiopoulos, et al., Ultrasmooth organic–inorganic perovskite thin-film formation and crystallization for efficient planar heterojunction solar cells, Nat. Commun. 6 (2015) 6142. http://dx.doi.org/10.1038/ncomms7142.
[8] W. Qiu, U.W. Paetzold, R. Gehlhaar, V. Smirnov, H.-G. Boyen, J.G. Tait, et al., Electron beam evaporated TiO2 layer for high efficiency planar perovskite solar cells on flexible polyethylene terephthalate substrates, J. Mater. Chem. A (2015) http://dx.doi.org/10.1039/C5TA07515G.
[9] N.J. Jeon, J.H. Noh, Y.C. Kim, W.S. Yang, S. Ryu, S. Il Seok, Solvent engineering for high-performance inorganic-organic hybrid perovskite solar cells, Nature Mater. 13 (2014) 1–7. http://dx.doi.org/10.1038/nmat4014.
[10] W.H. Nguyen, C.D. Bailie, E.L. Unger, M.D. McGehee, Enhancing the hole-conductivity of spiro-OMeTAD without oxygen or lithium salts by using spiro(TFSI)2 in perovskite and dye-sensitized solar cells, J. Am. Chem. Soc. 136 (2014) 10996–11001. http://dx.doi.org/10.1021/ja504539w.
[11] T.J. Jacobsson, L.J. Schwan, M. Ottosson, A. Hagfeldt, T. Edvinsson, Determination of thermal expansion coefficients and locating the temperature-induced phase transition in methylammonium lead perovskites using X-ray diffraction, Inorg. Chem. 54 (2015) 10678–10685. http://dx.doi.org/10.1021/acs.inorgchem.5b01481.
[12] X. Li, M.I. Dar, C. Yi, J. Luo, M. Tschumi, S.M. Zakeeruddin, et al., Improved performance and stability of perovskite solar cells by crystal crosslinking with alkylphosphonic acid ω-ammonium chlorides, Nature Chem. 7 (2015) 703–711. http://dx.doi.org/10.1038/nchem.2324.
[13] Y. Zhao, J. Wei, H. Li, Y. Yan, W. Zhou, D. Yu, et al., A polymer scaffold for self-healing perovskite solar cells, Nature Commun. 7 (2016) 10228. http://dx.doi.org/10.1038/ncomms10228.
[14] S. Yang, Y. Wang, P. Liu, Y.-B. Cheng, H.J. Zhao, H.G. Yang, Functionalization of perovskite thin films with moisture-tolerant molecules, Nat. Energy 1 (2016) 15016. http://dx.doi.org/10.1038/nenergy.2015.16.
[15] J. Xu, O. Voznyy, R. Comin, X. Gong, G. Walters, M. Liu, et al., Crosslinked remote-doped hole-extracting contacts enhance stability under accelerated lifetime testing in perovskite solar cells, Adv. Mater. (2016) 2807–2815. http://dx.doi.org/10.1002/adma.201505630.
[16] C. Bruner, N.C. Miller, M.D. McGehee, R.H. Dauskardt, Molecular intercalation and cohesion of organic bulk heterojunction photovoltaic devices, Adv. Funct. Mater. 23 (2013) 2863–2871. http://dx.doi.org/10.1002/adfm.201202969.
[17] M.F. Kanninen, An augmented double cantilever beam model for studying crack propagation and arrest, Int. J. Fract. 9 (1973) 83–92. http://dx.doi.org/10.1007/BF00035958.
[18] M. Saliba, S. Orlandi, T. Matsui, S. Aghazada, M. Cavazzini, J.-P. Correa-Baena, et al., A molecularly engineered hole-transporting material for efficient perovskite solar cells, Nat. Energy 1 (2016) 15017. http://dx.doi.org/10.1038/nenergy.2015.17.
[19] V. Balcaen, N. Rolston, S.R. Dupont, E. Voroshazi, R.H. Dauskardt, Thermal cycling effect on mechanical integrity of inverted polymer solar cells, Sol. Energy Mater. Sol. Cells 143 (2015) 418–423. http://dx.doi.org/10.1016/j.solmat.2015.07.019.
[20] S.R. Dupont, E. Voroshazi, P. Heremans, R.H. Dauskardt, The effect of anneal, solar irradiation and humidity on the adhesion/cohesion properties of P3HT:PCBM based inverted polymer solar cells, in: Conf. Rec. IEEE Photovolt. Spec. Conf., 2012: pp. 3259–3262. http://dx.doi.org/10.1109/PVSC.2012.6318272.
[21] S.R. Dupont, M. Oliver, F.C. Krebs, R.H. Dauskardt, Interlayer adhesion in roll-to-roll processed flexible inverted polymer solar cells, Sol. Energy Mater. Sol. Cells 97 (2012) 171–175. http://dx.doi.org/10.1016/j.solmat.2011.10.012.
[22] C. Bruner, F. Novoa, S. Dupont, R.H. Dauskardt, Decohesion kinetics in polymer organic solar cells, ACS Appl. Mater. Interfaces 6 (2014) 21474–21483. http://dx.doi.org/10.1021/am506482q.
[23] J.P. Hirth, The influence of grain boundaries on mechanical properties, Metall. Trans. 3 (1972) 3047–3067. http://dx.doi.org/10.1007/BF02661312.
[24] R.W. Rice, Microstructure Dependence of Mechanical Behavior of Ceramics, vol. 11, Academic Press Inc., 1977, pp. 199–381. http://dx.doi.org/10.1016/B978-0-12-341811-1.50010-8.
[25] J.H. Yun, I. Lee, T.-S. Kim, M.J. Ko, J.Y. Kim, H.J. Son, Synergistic enhancement and mechanism study of mechanical and moisture stability of perovskite solar cell introducing polyethyleneimine into CH3NH3PbI3/HTM Interface, J. Mater. Chem. A (2015) 22176–22182. http://dx.doi.org/10.1039/C5TA06008G.
[26] P. Brown, D. Thomas, A. Köhler, J. Wilson, J.-S. Kim, C. Ramsdale, et al., Effect of interchain interactions on the absorption and emission of poly(3-hexylthiophene), Phys. Rev. B 67 (2003) 1–16. http://dx.doi.org/10.1103/PhysRevB.67.064203.
[27] T. Malinauskas, D. Tomkute-Luksiene, R. Sens, M. Daskeviciene, R. Send, H. Wonneberger, et al., Enhancing thermal stability and lifetime of solid-state dye-sensitized solar cells via molecular engineering of the hole-transporting material spiro-OMeTAD, ACS Appl. Mater. Interfaces 7 (2015) 11107–11116. http://dx.doi.org/10.1021/am5090385.
[28] G. Niu, X. Guo, L. Wang, Review of recent progress in chemical stability of perovskite solar cells, J. Mater. Chem. A 2 (2015) 1–11. http://dx.doi.org/10.1039/C4TA04994B.
[29] G. Divitini, S. Cacovich, F. Matteocci, L. Cinà, A. Di Carlo, C. Ducati, In situ observation of heat-induced degradation of perovskite solar cells, Nat. Energy 1 (2016) 15012. http://dx.doi.org/10.1038/nenergy.2015.12.
[30] Y. Han, S. Meyer, Y. Dkhissi, K. Weber, J.M. Pringle, U. Bach, et al., Degradation observations of encapsulated planar CH3NH3PbI3 perovskite solar cells at high temperatures and humidity, J. Mater. Chem. A. 3 (2015) 8139–8147. http://dx.doi.org/10.1039/C5TA00358J.
[31] H.L. Clever, F.J. Johnston, The solubility of some sparingly soluble lead salts: An evaluation of the solubility in water and aqueous electrolyte solution, J. Phys. Chem. Ref. Data 9 (1980) 751. http://dx.doi.org/10.1063/1.555628.
[32] R. Ghosh Chaudhuri, S. Paria, Core/shell nanoparticles: Classes, properties, synthesis mechanisms, characterization, and applications, Chem. Rev. 112 (2012) 2373–2433. http://dx.doi.org/10.1021/cr100449n.